
HyPlaneHead: Rethinking Tri-plane-like Representations in Full-Head Image Synthesis

Heyuan Li*

SSE, CUHK (Shenzhen)

heyuanli@link.cuhk.edu.cn

Kenkun Liu

SSE, CUHK (Shenzhen)

kenkunli@link.cuhk.edu.cn

Lingteng Qiu†

Tongyi Lab, Alibaba Inc.

qiulingteng qlt@alibaba-inc.com

Qi Zuo

Tongyi Lab, Alibaba Inc.

muyuan.zq@alibaba-inc.com

Keru Zheng

SSE, CUHK (Shenzhen)

keruzheng@link.cuhk.edu.cn

Zilong Dong

Tongyi Lab, Alibaba Inc.

list.dzl@alibaba-inc.com

Xiaoguang Han‡

SSE, CUHK (Shenzhen)

hanxiaoguang@cuhk.edu.cn

Abstract

Tri-plane-like representations have been widely adopted in 3D-aware GANs for head image synthesis and other 3D object/scene modeling tasks due to their efficiency. However, querying features via Cartesian coordinate projection often leads to feature entanglement, which results in mirroring artifacts. A recent work, SphereHead, attempted to address this issue by introducing spherical tri-planes based on a spherical coordinate system. While it successfully mitigates feature entanglement, SphereHead suffers from uneven mapping between the square feature maps and the spherical planes, leading to inefficient feature map utilization during rendering and difficulties in generating fine image details. Moreover, both tri-plane and spherical tri-plane representations share a subtle yet persistent issue: feature penetration across convolutional channels can cause interference between planes, particularly when one plane dominates the others (see fig. 1). These challenges collectively prevent tri-plane-based methods from reaching their full potential. In this paper, we systematically analyze these problems for the first time and propose innovative solutions to address them. Specifically, we introduce a novel hybrid-plane (hy-plane for short) representation that combines the strengths of both planar and spherical planes while avoiding their respective drawbacks. We further enhance the spherical plane by replacing the conventional theta-phi warping with a novel near-equal-area warping strategy, which maximizes the effective utilization of the square feature map. In addition, our generator synthesizes a single-channel unified feature map instead of multiple feature maps in separate channels, thereby effectively eliminating feature penetration. With a series of technical improvements, our hy-plane representation enables our method, HyPlaneHead, to achieve state-of-the-art performance in full-head image synthesis.

*Work done during an internship at Tongyi Lab, Alibaba Inc.

†Project lead.

‡Corresponding author.

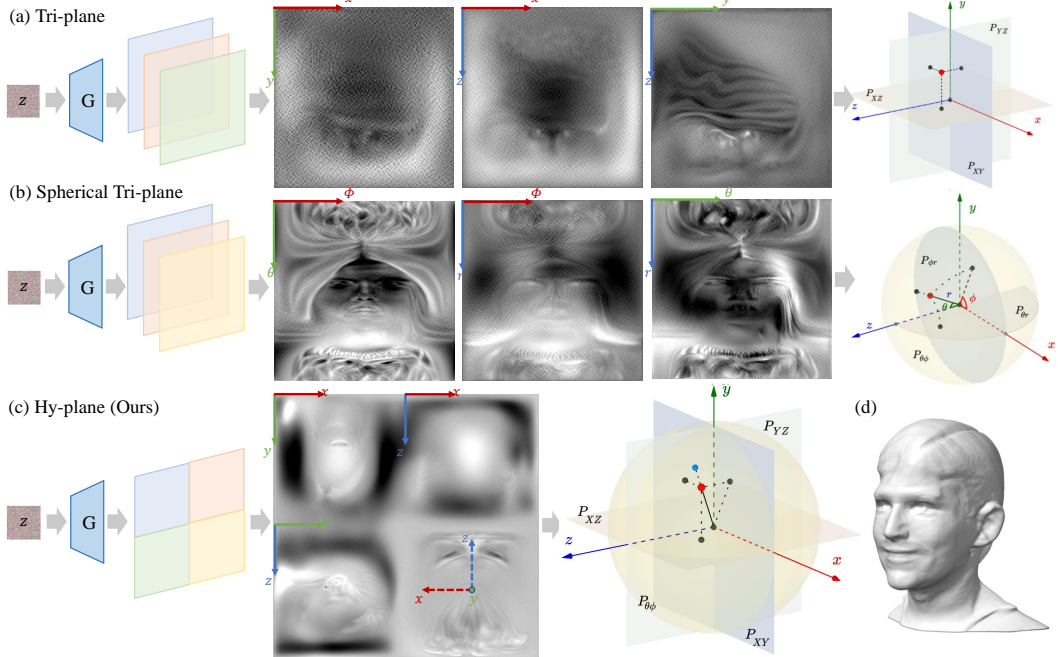


Figure 1: Figure (a, b, c) respectively illustrate the feature map visualizations and geometric structures of the tri-plane, spherical tri-plane, and our proposed hy-plane representation which integrates both planar and spherical planes. Figure (d) shows a head geometry model for defining the coordinate system. Note that in (a, b), the dominant planes (P_{YZ} for tri-plane and $P_{\theta\phi}$ for spherical tri-plane) cause significant inter-channel feature penetration into the other two planes (best viewed when zoomed in), thereby limiting the model’s expressiveness. In contrast, (c) resolves this issue entirely by employing a unify-split strategy, where all feature maps are generated within a single channel. As a result, each plane effectively learns its corresponding information without interference from other planes.

1 Introduction

Photorealistic full-head synthesis Zhuang et al. (2022); Park et al. (2021); Canela et al. (2023); He et al. (2024); Doukas et al. (2021) stands as a cornerstone technology for emerging applications in augmented/virtual reality avatars, immersive telepresence systems, and next-generation digital content creation. While modern 2D generative adversarial networks (GANs) Goodfellow et al. (2020); Radford et al. (2015); Mao et al. (2017); Gulrajani et al. (2017); Zhou et al. (2021); Kang et al. (2023) achieve remarkable image quality in frontal face generation, their fundamental limitation in 3D scene modeling becomes apparent when synthesizing head images under arbitrary viewpoints.

Recent advancements in 3D-aware GANs Schwarz et al. (2020); Deng et al. (2022); Xue et al. (2022); Nguyen-Phuoc et al. (2019); Chan et al. (2021); Shi et al. (2021); Chan et al. (2022); An et al. (2023); Li et al. (2024) have tackled this challenge by leveraging neural implicit representations, enabling view-consistent synthesis while maintaining photorealistic quality. Among these methods, the pioneering work EG3D Chan et al. (2022) employs a tri-plane structure to represent human heads or other 3D objects. The tri-plane representation Gao et al. (2022); Shue et al. (2023); Zou et al. (2024); Wang et al. (2023b); Hong et al. (2023); Gupta et al. (2023); Zuo et al. (2023); Wu et al. (2024); Zuo et al. (2024) efficiently captures symmetrical regions because two 3D points that are symmetric with respect to a feature plane will query the same feature on the plane via Cartesian coordinate projection. However, this inherent coupling of features becomes problematic in asymmetrical areas, leading to mirroring artifacts. As shown in fig. 2 (a, b), a typical example in full-head synthesis is that the back-view of the head shares the same features on the F_{xy} plane as the front-view face, resulting in noticeable fake face artifacts on the back of the head. While PanoHead An et al. (2023) mitigates this issue by augmenting each plane with additional parallel planes, its tri-grid representation does not fundamentally resolve the problem, as it still inherits the same geometric and projection limitations of the Cartesian coordinate system.

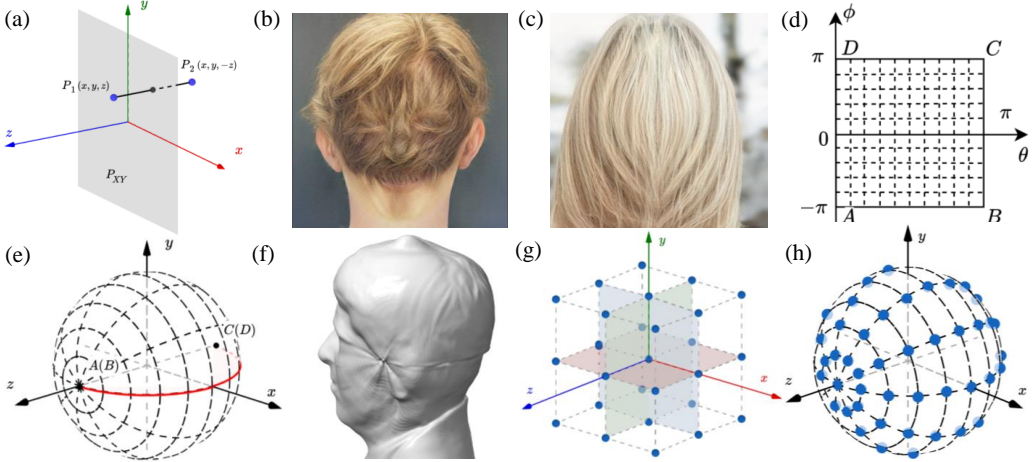


Figure 2: In the tri-plane representation, (a) the feature entanglement issue results in mirroring artifacts, where (b) the back of the head incorrectly exhibits front-face attributes, or (c) the hair’s texture and shape display an unnaturally high degree of left-right symmetry. In the spherical tri-plane representation, (d, e) the non-equal-area warping caused by mapping a square to a sphere using (θ, ϕ) coordinates introduces (f) artifacts in the seam and polar regions, as well as uneven spatial feature distribution after warping. By contrast, (g) the tri-plane representation exhibits even spatial feature distribution, whereas (h) the spherical tri-plane representation shows uneven distribution, with features being overly dense in the polar regions and sparse near the equator.

A recent work, SphereHead Li et al. (2024), creatively addresses the mirroring issue by introducing a spherical tri-plane representation that projects features in a spherical coordinate system. However, this approach introduces new challenges. First, it fails to leverage symmetry, which is prevalent in real-world objects. Second, the mapping from the square feature map to the spherical plane $F_{\theta\phi}$ involves a non-equal-area projection. Specifically, as illustrated in fig. 2 (c-f), after this mapping, features are sparsest near the equator and densest at the poles. This uneven distribution results in inefficient feature map utilization when rendering 2D images, reducing the model’s ability to capture fine details. Moreover, referring to fig. 2 (d), a single spherical tri-plane can produce artifacts in the seam region due to the numerical discontinuity of $F_{\theta\phi}$ at $\phi = -\pi$ and $\phi = \pi$ in the spherical coordinate system. Although SphereHead mitigates this issue by incorporating an additional orthogonal spherical tri-plane, this solution complicates the model and introduces parameter redundancy. Worse still, the least expressive equatorial region of one sphere are used to cover the most expressive polar regions of the other, further diminishing the overall expressiveness of the representation.

Besides, we are the first to observe that a subtle yet persistent issue exists in both tri-plane and spherical tri-plane representations: feature penetration across convolutional channels can lead to interference between feature planes, particularly when one plane dominates the others. This issue arises because, unlike RGB images where channels are spatially aligned in 2D, each feature plane has a unique distribution, resulting in significantly different spatial meaning and values at the same uv position. In convolutional layers, however, all output channels at a given uv position are computed using the same input values. Ideally, the network is supposed to learn appropriate kernels to separate information for different planes. Yet, this is particularly challenging for 3D-aware GANs, as they are trained on 2D images Niemeyer and Geiger (2021) without direct supervision on feature maps. Consequently, feature penetration often manifests visibly across planes, as shown in fig. 1. Although visible feature penetration gradually diminishes as training progresses, the issue itself remains difficult to fully resolve, subtly limiting the model’s expressiveness and causing seemingly inexplicable artifacts.

In this paper, we introduce a simple yet effective **unify-split strategy** that generates a single-channel feature map and then splits it into multiple feature planes, instead of using different output channels to generate different feature planes. This approach completely eliminates the issue of feature penetration between channels. Building on this, we propose a novel **hy-plane (hy-plane) representation** that integrates both planar and spherical feature planes, as illustrated in fig. 1 (c). This design leverages the strengths of both tri-plane and spherical tri-plane representations while mitigating their

respective limitations. Specifically, the hy-plane representation automatically learns symmetrical features using planar planes and captures anisotropic features through the spherical plane. This approach avoids mirroring artifacts while ensuring a uniformly high feature density throughout 3D rendering. Furthermore, to optimize the mapping from the square feature map to the spherical plane, we employ Lambert azimuthal equal-area projection Özürk (2024) combined with elliptical grid mapping Fong (2019). These techniques maximize the utilization of the square feature map and eliminate the seam artifacts. We also explore several variant models to further enhance performance. For instance, we increase the area proportion of the spherical plane to boost its expressive power and propose a dual-plane-dual-sphere variant to fully resolve polar artifacts. These innovations collectively contribute to the robustness and versatility of our hy-plane representation.

Building on the aforementioned technical advancements, the novel hy-plane representation enables our **HyPlaneHead** model to achieve state-of-the-art performance in full-head image synthesis, delivering high-quality results with significantly fewer artifacts compared to existing 3D-aware GAN methods Schwarz et al. (2020); Deng et al. (2022); Xue et al. (2022); Nguyen-Phuoc et al. (2019); Chan et al. (2021); Shi et al. (2021); Chan et al. (2022); An et al. (2023); Li et al. (2024). In summary, our main contributions are as follows:

- We conduct an in-depth analysis of the limitations inherent in tri-plane-like representations used in 3D-aware GANs. Based on this understanding, we introduce the *hy-plane representation*, which combines the strengths of both planar and spherical planes while addressing their respective drawbacks.
- To achieve seamless integration of planar and spherical planes, we propose a series of technical innovations, including *unify-split strategy*, a novel *near-equal-area warping* method, *area-biased splitting*, and exploration of *alternative combination strategies*.
- Through comprehensive experiments, we validate the effectiveness of our proposed representation. Our *HyPlaneHead* model achieves state-of-the-art performance for full-head image synthesis, demonstrating superior quality and reduced artifacts.

2 Related Work

3D Morphable Head Representations. Traditional approaches for representing 3D faces with diverse shapes and appearances rely on 3D Morphable Models (3DMM) Blanz and Vetter (1999); Paysan et al. (2009), with FLAME Li et al. (2017) extending this framework to full head modeling. However, the coarse geometric details provided by 3DMMs have motivated numerous works to combine them with implicit neural representations, such as NeRF Caneja et al. (2023); Zanfir et al. (2022); Zheng et al. (2022); Gafni et al. (2021); Guo et al. (2021); Park et al. (2021); Wu et al. (2023a); Yenamandra et al. (2021); Zhang et al. (2023); Zhuang et al. (2022). While volume-based rendering techniques have significantly enhanced the capabilities of 3DMM-based models, their inherent topological constraints limit the expressiveness of implicit representations, particularly in capturing fine details like hair and wrinkles. Consequently, recent 3D-aware generative models have shifted towards directly synthesizing implicit neural fields of heads without relying on 3DMM priors.

Generative Neural Head Representations. Emerging neural head generative models Nguyen-Phuoc et al. (2020); Schwarz et al. (2020); Deng et al. (2022); Chan et al. (2021); Shi et al. (2021); Nguyen-Phuoc et al. (2019); Xue et al. (2022) adopt 3D-aware representations Mildenhall et al. (2021) which can be optimized by multi-view images through differentiable rendering. Though these implicit representations offer potential memory efficiency and structure complexity compared with traditional 3DMM-based representations Paysan et al. (2009); Blanz and Vetter (1999); Li et al. (2017). Query-based feature sampling and fully connected mapping slow down the convergence process. To maintain representation complexity while accelerate the optimization process, EG3D Chan et al. (2022) proposes tri-plane representation to explicitly store features on axis-aligned planes that are aggregated by a lightweight implicit feature decoder for efficient volume rendering. However, inherent coupling of features and mirroring issue are also brought with the efficiency. PanoHead An et al. (2023) propose to exploit extra in-the-wild data to supervise the back of head, thus can generate views in 360° full head setting. Although it enriches the tri-plane’s representational capacity through adding more parallel feature planes, PanoHead can not thoroughly solve the mirroring issue from representation level. SphereHead Li et al. (2024), through a shift in formulation from a Cartesian coordinate representation in cubic space to a spherical coordinate representation in spherical space,

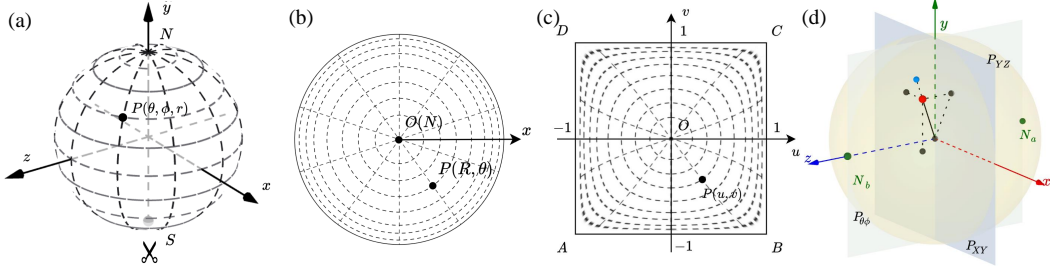


Figure 3: (a) The Lambert azimuthal equal-area projection (LAEAs) opens the South Pole, and maps the sphere to (b) a flat circular plane, with the North Pole at its center. (c) Elliptical grid mapping transforms the circular plane into a square. Conversely, the square can be inversely mapped back to a sphere with near-equal-area properties. (d) In the hy-plane (2+2) representation, two spheres coincide, with their North Poles facing in opposite directions. Please refer to the supplementary videos for a more comprehensive understanding.

greatly eliminates the mirroring issue and avoids many artifacts. While SphereHead Li et al. (2024) addresses many limitations of prior work, it fails to preserve the simplicity of representing symmetric objects and introduces discontinuities along the seam between the two poles. To this end, we propose a novel *hy-plane representation* that effectively represents both symmetric and asymmetric regions, eliminates the mirroring issue, and avoids representation discontinuity.

3 Method

3.1 Hy-Plane Representation

As illustrated in fig. 2, both tri-plane and spherical tri-plane have distinct strengths and limitations. The tri-plane representation benefits from uniform and dense spatial feature distribution, enabled by Cartesian coordinate projection. It efficiently renders high-resolution images from various angles and leverages symmetry effectively. However, it struggles with disentangling asymmetric features, leading to unwanted mirroring artifacts caused by feature entanglement. In contrast, the spherical tri-plane uses spherical coordinate projection to naturally distinguish directional features and learn anisotropic representations, avoiding feature entanglement. Yet, its non-uniform feature distribution reduces feature map utilization and complicates the rendering of high-resolution details.

Recognizing the complementary nature of these approaches, we propose *hy-plane*, a novel hybrid representation combining planar and spherical planes. hy-plane uses planar components to capture symmetric features and spherical components to model anisotropic features. This design retains the efficiency and uniformity of the tri-plane while eliminating feature entanglement and mirroring artifacts.

Hy-Plane (3+1) The basic version of our representation consists of three planar planes plus one spherical plane, referred to as hy-plane (3+1). The three planar planes are arranged mutually orthogonally, with the positive z-axis aligned toward the human face, the positive y-axis pointing to the top of the head, and the positive x-axis directed toward the left ear. Features are queried using Cartesian coordinate projection. The spherical plane adopts a spherical coordinate system, with the polar axis aligned with the head’s top direction. Notably, instead of directly querying the feature map using (θ, ϕ) coordinates, we employ a novel *near-equal-area warping* method to improve feature map utilization.

Near-Equal-Area Warping Directly querying the feature map using (θ, ϕ) coordinates, as in spherical tri-plane, is straightforward but introduces significant side effects. Geometrically (fig. 2(c,d)), wrapping a square feature map $P_{\theta\phi}$ into a spherical plane causes numerical discontinuities at $\phi = -\pi$ and $\phi = \pi$, leading to artifacts in the seam region. Additionally, the edges $\theta = 0$ and $\theta = \pi$ contract into polar points, converting fluctuations along these lines into high-frequency noise around the poles. Furthermore, this warping is non-equal-area, unevenly distributing features from the square feature map onto the sphere. The equator region becomes feature-sparse, reducing expressive ability, while the poles become feature-dense, causing polar artifacts. Although SphereHead Li et al. (2024) addresses seam and polar artifacts by introducing an orthogonal dual-sphere setup, this approach

doubles the number of feature planes but compromises the model’s overall expressiveness, because each sphere uses its feature-sparse equator region to cover the other’s feature-dense polar regions, further limiting representation quality.

To address the challenging wrapping problem, we propose an elegant solution based on Lambert azimuthal equal-area projection (LAEA projection):

$$(R, \Theta) = \left(2 \cos \frac{1}{2} \phi, -\theta \right), \quad (1)$$

where (θ, ϕ) denote colatitude and longitude in spherical coordinates on the spherical feature plane, and (R, Θ) denote radius and azimuth in polar coordinates on the flatten circle feature map. As shown in fig. 3 (a, b), LAEA projection unfolds the spherical surface from the South Pole and flattens it into a circular plane centered on the North Pole. This method ensures equal-area transformation by adaptively adjusting latitudinal line density along the radius, achieving uniform feature distribution during warping. Additionally, it consolidates the seam and two poles of the spherical coordinate system into a single point, making them easier to handle. We align this point with the downward direction of the 3D head, which remains invisible in the rendering.

Next, we use elliptical grid mapping to transform the circle into a square, as illustrated in fig. 3 (b, c), which can be formulated as follows:

$$(x, y) = (R \cos \Theta, R \sin \Theta), \quad (2)$$

$$\begin{cases} u = \frac{1}{2} \sqrt{2 + x^2 - y^2 + 2\sqrt{2}x} - \frac{1}{2} \sqrt{2 + x^2 - y^2 - 2\sqrt{2}x}, \\ v = \frac{1}{2} \sqrt{2 - x^2 + y^2 + 2\sqrt{2}y} - \frac{1}{2} \sqrt{2 - x^2 + y^2 - 2\sqrt{2}y}. \end{cases} \quad (3)$$

where (x, y) are coordinates on the circle, and (u, v) are coordinates on the square feature map. This near-equal-area mapping minimizes severe deformation, preserving feature quality. When querying a 3D point’s feature on the spherical plane, we first convert its spherical coordinates (θ, ϕ) to polar coordinates (R, Θ) on the wrapped circle using eq. (1). We then transform these polar coordinates into 2D Cartesian coordinates (x, y) via eq. (2), and finally map them to the corresponding (u, v) location on the square feature map using eq. (3). This approach maximizes the utilization of the feature map while effectively eliminating seam artifacts.

Hy-Plane (2+2) While in human head modeling, we can hide the final pole (the South Pole) by orienting it downward, this approach may not be applicable to other scenes or objects where no such unimportant direction exists for hiding. This limits its broader applicability. To address this, we introduce hy-plane (2+2), a variant consisting of two orthogonal planar planes and two spherical planes with opposing poles. When querying a 3D point’s feature on the spherical planes, we compute features separately and combine them using a weighting function:

$$\begin{cases} w_a = (R_a^{\max} - R_a)^2, \\ w_b = (R_b^{\max} - R_b)^2, \\ f_{\text{sph}} = \frac{w_a f_a + w_b f_b}{w_a + w_b} \end{cases} \quad (4)$$

Here, R_a and R_b represent the radii of the 3D point projected onto the two wrapped circles. R_a^{\max} and R_b^{\max} denote the radii of the circles. The weights w_a and w_b are inversely proportional to these radii, peaking at the center ($R = 0$) and decreasing toward the edges ($R = R^{\max}$). This design optimizes the use of the feature map’s flat central region while minimizing the impact of the distorted edge areas, effectively resolving artifacts at the poles.

The reason for reducing one planar plane while adding a spherical plane is to be compatible with the unify-split strategy, as will be explained in section 3.2. Notably, as demonstrated in Wang et al. (2023a), two orthogonal planar planes can function nearly identically to three, since any two planes (P_{XY}, P_{XZ}, P_{YZ}) encompass all three coordinates (x, y, z) .

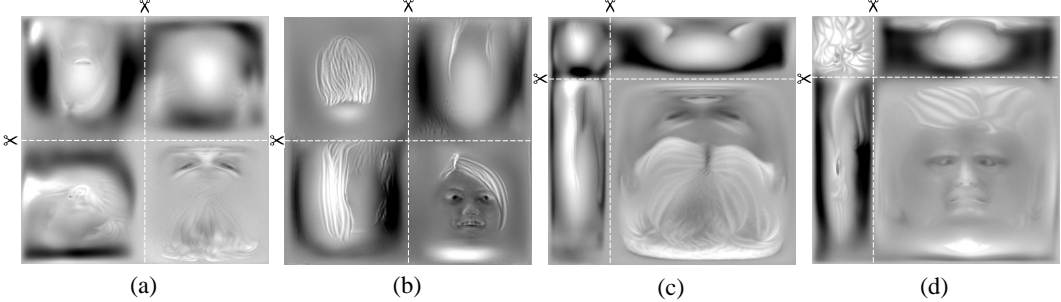


Figure 4: Unify-Split Strategy. (a) Hy-plane (3+1) with evenly splitting; (b) Hy-plane (2+2) with evenly splitting; (c) Hy-plane (3+1) with area-biased splitting; (d) Hy-plane (2+2) with area-biased splitting.

3.2 Unify-Split Strategy

Feature Penetration across Channels A key reason for the widespread adoption of tri-plane-like representations is their ability to represent 3D objects using 2D feature planes, whose data structure is similar to 2D images. This allows researchers to directly leverage existing 2D image generation architectures for 3D-aware object synthesis. However, reusing these models directly, without adapting to the inherent differences between 2D RGB images and 3D-aware tri-plane-like representations, leads to a critical oversight. In RGB images, the three channels represent different colors but share the same 2D spatial context. That is, the same uv position corresponds to the same spatial location, with only color variations across channels. This creates strong correlations during neural network training, enabling the network to first learn shared features layer by layer and then separate them into individual channels at the final output layer.

In contrast, in tri-plane-like representations, each plane encodes features from different spatial directions. Consequently, the same uv position on different planes corresponds to entirely distinct spatial meanings. Forcing convolutional networks to learn unrelated features at identical uv positions across planes increases learning complexity and causes feature entanglement between disparate spatial locations. This issue is particularly pronounced in 3D-aware GANs, where the model indirectly optimizes feature planes by learning from 2D images. The difficulty in disentangling information across feature planes leads to visible interference between output channels, resulting in unexpected artifacts in the generated images.

Evenly Splitting Based on the aforementioned observation, we adopt a simple yet effective *unify-split strategy* for synthesizing tri-plane-like representations. Instead of using separate channels for different feature planes, we allocate distinct regions on a large unified one-channel feature plane and then split it into parts corresponding to individual feature planes. This spatially disentangles features across planes in 2D space. fig. 4 (a, b) illustrates the splitting process for hy-plane (3+1) and hy-plane (2+2), where all four planes are evenly divided into two-by-two configurations.

Area-Biased Splitting Additionally, we can refine the 2D splitting scheme to enhance specific capabilities of the hy-plane. For instance, in full-head synthesis, the ability to model anisotropic features is crucial for generating high-resolution back-head details. As shown in fig. 4(c, d), for hy-plane (3+1), we increase the area of the spherical plane and elongate the feature maps P_{XY} and P_{YX} along different axes. This maximizes their expressive power when combined. For hy-plane (2+2), we enlarge one primary spherical plane while shrinking the other. The larger plane remains a full sphere, while the smaller one forms a spherical cap, covering the problematic polar region of the larger sphere.

3.3 HyPlaneHead

We integrate our hy-plane representation into HyPlaneHead, a 3D-aware GAN pipeline akin to Chan et al. (2022); An et al. (2023); Li et al. (2024). Given a sampled z and conditioned camera parameter c_{con} , the generator G produces a one-channel unified feature map, which is then split into individual feature planes of the hy-plane representation. Features are queried from each plane and volumetrically rendered using the viewing camera c_{ren} , enabling HyPlaneHead to generate a head image I and



Figure 5: Qualitative comparison with state-of-the-art methods. (a) Tri-plane representation from Chan et al. (2022). (b) Tri-grid representation from An et al. (2023). (c) Single spherical tri-plane representation from Li et al. (2024), where the white dashed box highlights a discontinuity in the hair region. (d, e) Dual spherical tri-plane representation from Li et al. (2024). (f–j) Our proposed Hy-plane representation. A closer inspection is recommended for finer details, and we refer readers to the supplementary material for higher-resolution visualizations.

mask I^m . As in Chan et al. (2022); An et al. (2023); Li et al. (2024), the output passes through a super-resolution module to produce the high-resolution head image I^+ . Following An et al. (2023); Li et al. (2024), we also introduce a background generator to allow G to focus specifically on the head region. In addition to the conventional 3D-aware GAN losses used in Chan et al. (2022), we further employ a view-image consistency loss, as proposed in Li et al. (2024), to guide the discriminator to focus on the alignment between images and their corresponding viewpoints.

4 Experiments

In this section, we conduct comprehensive qualitative and quantitative experiments on full-head image synthesis to demonstrate that our hy-plane representation is well-suited for rendering from any viewpoint. Our comparative analysis includes tri-plane, tri-grid, spherical tri-plane from EG3D, PanoHead, SphereHead respectively, and various hy-plane variants and settings for ablation study, all trained on our dataset and pipeline. All experiments are trained on eight NVIDIA V100 GPUs with a batch size of 32. We follow PanoHead and SphereHead, using a training set that includes FFHQ Niemeyer and Geiger (2021), CelebA Liu et al. (2018), LPFF Wu et al. (2023b), WildHead Li et al. (2024), K-Hairstyle Kim et al. (2021), and a 6K in-house dataset of large-pose head images processed with SphereHead’s toolbox. All training images are 512×512 in resolution and augmented with horizontal flips. The entire training process spans 25 million images.

4.1 Qualitative Comparison

We visualized synthesized samples and feature planes under varying configurations. For feature plane analysis, channel activations were averaged across feature-dimensions to visualize spatial texture patterns. As shown in fig. 1(a,b), tri-plane and spherical tri-plane models exhibit notable cross-plane interference: secondary feature maps show identical texture patterns from the dominating plane, alongside anomalous noise pattern. We suspect this phenomenon arises from inter-channel feature penetration, where competing planes disrupt each other’s activations. Contrastingly, our unify-split strategy (fig. 1(c)) allows each plane to specialize in its directional features without cross-channel interference, thereby producing informative and clear feature maps. From fig. 1 (c) and fig. 4, our hy-plane representation effectively integrates planar and spherical planes, enabling seamless collaboration through a division of labor. The planar planes specialize in capturing symmetric

Table 1: Quantitative comparison on Full-head Image Synthesis task. We list FID, FID-random metrics with different representations. * denote that we output two spherical tri-planes simultaneously by a shared branch.

No.	Representation	Unify-Split	Wrapping	FID	FID-random
1	Tri-plane (EG3D Chan et al. (2022))	-	-	9.22	11.23
2	Tri-plane	evenly split	-	8.86	11.52
3	Spherical Tri-plane (SphereHead Li et al. (2024))	-	-	8.64	10.71
4	Spherical Tri-plane	evenly split	-	8.36	10.42
5	Dual Spherical Tri-plane	-	-	8.68	10.28
6	Dual Spherical Tri-plane *	-	-	11.9	13.54
7	Tri-grid (PanoHead An et al. (2023))	-	-	8.77	10.66
8	Tri-plane 512^2	-	-	9.27	10.89
9	Spherical Tri-plane 512^2	-	-	8.82	10.47
10	Tri-grid 512^2	-	-	8.79	10.78
11	Hy-plane (3+1)	-	-	8.54	10.66
12	Hy-plane (3+1)	evenly split	-	8.31	10.18
13	Hy-plane (3+1)	evenly split	yes	8.18	9.96
14	Hy-plane (3+1)	area-bias split	yes	8.14	9.88
15	Hy-plane (2+2)	evenly split	yes	8.28	10.01
16	Hy-plane (2+2)	area-bias split	yes	8.17	9.84

features (e.g., P_{YZ} learns left-right symmetric details such as side hair, ears, and shoulders), while the spherical plane excels at modeling anisotropic features (e.g., the frontal face and back-view hair).

fig. 5 compares our method with state-of-the-art full-head 3D-aware GANs. (a) The tri-plane representation from Chan et al. (2022), retrained on our dataset, generates mirrored faces at the back due to feature entanglement. (b) PanoHead An et al. (2023) uses a tri-grid structure but still exhibits excessive symmetry in hairstyles. (c) The single spherical tri-plane from SphereHead Li et al. (2024) produces full-head geometry but introduces seam and polar artifacts via (θ, ϕ) warping. (d, e) Its dual spherical variant reduces artifacts but leads to over-smoothed textures and loss of detail. (f–j) Our HyPlaneHead combines planar and spherical representations, achieving high-quality synthesis with rich texture and geometric fidelity, setting a new benchmark for full-head 3D-aware GANs.

4.2 Quantitative Comparison and Ablation Study

To quantitatively evaluate the visual quality, fidelity, and diversity of the synthesized full-head images, we employed the Frechet Inception Distance (FID) metric Szegedy et al. (2016) on 50K real and synthetic samples. As noted in prior 3D-aware GANs based full-head image synthesis works An et al. (2023); Li et al. (2024), current 3D-aware GANs typically perform well under the conditioning camera pose during synthesis but degrade significantly at non-conditioned rendering angles. To rigorously assess performance under arbitrary viewing angles, which is especially critical for full-head image synthesis, we introduced a new evaluation metric, FID-random, which decouples the conditioning pose from the rendering pose. Specifically, during generation, we first randomly sample a camera parameter c_{con} from the dataset’s camera distribution to condition the tri-plane-like representation; subsequently, we render the head image using a different random camera parameter c_{ren} (also sampled from the same distribution). The FID score is then calculated based on the images rendered under these random viewpoints, thereby providing an unbiased evaluation of the model’s robustness and generalization across all possible angles.

Comparing table 1(1) with table 1(11) demonstrates the advantages of augmenting the tri-plane with a spherical plane, consistent with our earlier visualizations. The effectiveness of our unify-split strategy is evidenced by the general reduction in FID and FID-random scores across table 1(1,2,3,4,11,12). Notably, while applying the unify-split strategy to the tri-plane reduces FID, it increases FID-random. This occurs because the strategy eliminates inter-channel feature penetration, allowing each plane to fully express its directional features. However, since the tri-plane does not separate directional features, the enhanced plane expression exacerbates mirroring artifacts on the backside, thereby worsening FID-random. In contrast, both the spherical tri-plane and hy-plane benefit from the separation of directional features provided by the spherical plane, enabling them to leverage the improved expressiveness unlocked by the unify-split strategy, resulting in reductions in both FID and FID-random. table 1(3,4,5,6,9) reveal that directly outputting dual spherical tri-planes leads to significant interference between the two dominant theta-phi planes, yielding the highest FID

scores. SphereHead mitigates this issue by introducing two small convolution-based branches, albeit at the cost of increased parameters. However, adopting the unify-split strategy achieves superior results without additional parameters, as demonstrated by the single spherical tri-plane’s performance. table 1(12,13) validate that wrapping improves performance by fully utilizing the square feature map. In table 1(14,16), we split a 512×512 feature map into four parts via area-bias splitting: 384×384 , 384×128 , 384×128 , and 128×128 , with the largest allocated to the spherical plane. Comparing these configurations with table 1(13,15) confirms the effectiveness of this partitioning scheme for full-head synthesis. Finally, we tested the tri-plane, tri-grid, and spherical tri-plane with a feature map size of 512×512 . table 1(8,9,10) show minimal impact from increasing the feature map size, ruling out model parameter scaling as a significant factor influencing our experimental outcomes.

5 Conclusion

In this paper, we conduct an in-depth analysis of the limitations inherent in tri-plane-like representations used in 3D-aware GANs, particularly focusing on mirroring artifacts, uneven warping from the square feature map to the spherical plane, and feature penetration across channels. Based on these insights, we propose the hybrid-plane (hy-plane) representation, which combines the strengths of planar and spherical planes while mitigating their respective weaknesses. Our technical contributions include a unified planar-spherical representation, near-equal-area warping for seamless and efficient square-to-sphere mapping, and a unify-split strategy to eliminate feature penetration. These innovations enable HyPlaneHead to achieve state-of-the-art performance in full-head image synthesis, significantly reducing artifacts and enhancing rendering quality.

References

Sizhe An, Hongyi Xu, Yichun Shi, Guoxian Song, Umit Y Ogras, and Linjie Luo. Panohead: Geometry-aware 3d full-head synthesis in 360deg. In *Proceedings of the IEEE/CVF Conference on Computer Vision and Pattern Recognition*, pages 20950–20959, 2023.

Volker Blanz and Thomas Vetter. A morphable model for the synthesis of 3d faces. In *Proceedings of the 26th annual conference on Computer graphics and interactive techniques*, pages 187–194, 1999.

Antonio Canelà, Pol Caselles, Ibrar Malik, Gil Triginer Garces, Eduard Ramon, Jaime García, Jordi Sánchez-Riera, and Francesc Moreno-Noguer. Instantavatar: Efficient 3d head reconstruction via surface rendering. *arXiv preprint arXiv:2308.04868*, 2023.

Eric R Chan, Marco Monteiro, Petr Kellnhofer, Jiajun Wu, and Gordon Wetzstein. pi-gan: Periodic implicit generative adversarial networks for 3d-aware image synthesis. In *Proceedings of the IEEE/CVF conference on computer vision and pattern recognition*, pages 5799–5809, 2021.

Eric R Chan, Connor Z Lin, Matthew A Chan, Koki Nagano, Boxiao Pan, Shalini De Mello, Orazio Gallo, Leonidas J Guibas, Jonathan Tremblay, Sameh Khamis, et al. Efficient geometry-aware 3d generative adversarial networks. In *Proceedings of the IEEE/CVF Conference on Computer Vision and Pattern Recognition*, pages 16123–16133, 2022.

Yu Deng, Jiaolong Yang, Jianfeng Xiang, and Xin Tong. Gram: Generative radiance manifolds for 3d-aware image generation. In *Proceedings of the IEEE/CVF Conference on Computer Vision and Pattern Recognition*, pages 10673–10683, 2022.

Michail Christos Doukas, Stefanos Zafeiriou, and Viktoria Sharmancka. Headgan: One-shot neural head synthesis and editing. In *Proceedings of the IEEE/CVF International conference on Computer Vision*, pages 14398–14407, 2021.

Chamberlain Fong. Elliptification of rectangular imagery, 2019.

Guy Gafni, Justus Thies, Michael Zollhofer, and Matthias Nießner. Dynamic neural radiance fields for monocular 4d facial avatar reconstruction. In *Proceedings of the IEEE/CVF Conference on Computer Vision and Pattern Recognition*, pages 8649–8658, 2021.

Jun Gao, Tianchang Shen, Zian Wang, Wenzheng Chen, Kangxue Yin, Daiqing Li, Or Litany, Zan Gojcic, and Sanja Fidler. Get3d: A generative model of high quality 3d textured shapes learned from images. *Advances In Neural Information Processing Systems*, 35:31841–31854, 2022.

Ian Goodfellow, Jean Pouget-Abadie, Mehdi Mirza, Bing Xu, David Warde-Farley, Sherjil Ozair, Aaron Courville, and Yoshua Bengio. Generative adversarial networks. *Communications of the ACM*, 63(11): 139–144, 2020.

Ishaan Gulrajani, Faruk Ahmed, Martin Arjovsky, Vincent Dumoulin, and Aaron C Courville. Improved training of wasserstein gans. *Advances in neural information processing systems*, 30, 2017.

Yudong Guo, Keyu Chen, Sen Liang, Yong-Jin Liu, Hujun Bao, and Juyong Zhang. Ad-nerf: Audio driven neural radiance fields for talking head synthesis. In *Proceedings of the IEEE/CVF International Conference on Computer Vision*, pages 5784–5794, 2021.

Anchit Gupta, Wenhan Xiong, Yixin Nie, Ian Jones, and Barlas Oğuz. 3dgen: Triplane latent diffusion for textured mesh generation. *arXiv preprint arXiv:2303.05371*, 2023.

Yuxiao He, Yiyu Zhuang, Yanwen Wang, Yao Yao, Siyu Zhu, Xiaoyu Li, Qi Zhang, Xun Cao, and Hao Zhu. Head360: Learning a parametric 3d full-head for free-view synthesis in 360 $\{\backslash\deg\}$. *arXiv preprint arXiv:2408.00296*, 2024.

Yicong Hong, Kai Zhang, Juxiang Gu, Sai Bi, Yang Zhou, Difan Liu, Feng Liu, Kalyan Sunkavalli, Trung Bui, and Hao Tan. Lrm: Large reconstruction model for single image to 3d. *arXiv preprint arXiv:2311.04400*, 2023.

Minguk Kang, Jun-Yan Zhu, Richard Zhang, Jaesik Park, Eli Shechtman, Sylvain Paris, and Taesung Park. Scaling up gans for text-to-image synthesis. In *Proceedings of the IEEE/CVF conference on computer vision and pattern recognition*, pages 10124–10134, 2023.

Taewoo Kim, Chaeyeon Chung, Sunghyun Park, Gyojung Gu, Keonmin Nam, Wonzo Choe, Jaesung Lee, and Jaegul Choo. K-hairstyle: A large-scale korean hairstyle dataset for virtual hair editing and hairstyle classification. In *2021 IEEE International Conference on Image Processing (ICIP)*, pages 1299–1303. IEEE, 2021.

Heyuan Li, Ce Chen, Tianhao Shi, Yuda Qiu, Sizhe An, Guanying Chen, and Xiaoguang Han. Spherehead: stable 3d full-head synthesis with spherical tri-plane representation. In *European Conference on Computer Vision*, pages 324–341. Springer, 2024.

Tianye Li, Timo Bolkart, Michael J Black, Hao Li, and Javier Romero. Learning a model of facial shape and expression from 4d scans. *ACM Trans. Graph.*, 36(6):194–1, 2017.

Ziwei Liu, Ping Luo, Xiaogang Wang, and Xiaoou Tang. Large-scale celebfaces attributes (celeba) dataset. *Retrieved August, 15(2018):11*, 2018.

Xudong Mao, Qing Li, Haoran Xie, Raymond YK Lau, Zhen Wang, and Stephen Paul Smolley. Least squares generative adversarial networks. In *Proceedings of the IEEE international conference on computer vision*, pages 2794–2802, 2017.

Ben Mildenhall, Pratul P Srinivasan, Matthew Tancik, Jonathan T Barron, Ravi Ramamoorthi, and Ren Ng. Nerf: Representing scenes as neural radiance fields for view synthesis. *Communications of the ACM*, 65(1):99–106, 2021.

Thu Nguyen-Phuoc, Chuan Li, Lucas Theis, Christian Richardt, and Yong-Liang Yang. Hologan: Unsupervised learning of 3d representations from natural images. In *Proceedings of the IEEE/CVF International Conference on Computer Vision*, pages 7588–7597, 2019.

Thu H Nguyen-Phuoc, Christian Richardt, Long Mai, Yongliang Yang, and Niloy Mitra. Blockgan: Learning 3d object-aware scene representations from unlabelled images. *Advances in neural information processing systems*, 33:6767–6778, 2020.

Michael Niemeyer and Andreas Geiger. Campari: Camera-aware decomposed generative neural radiance fields. In *2021 International Conference on 3D Vision (3DV)*, pages 951–961. IEEE, 2021.

Emre Öztürk. Lambert azimuthal equal-area projection. *Eskişehir Technical University Journal of Science and Technology A-Applied Sciences and Engineering*, 25(3):380–389, 2024.

Keunhong Park, Utkarsh Sinha, Jonathan T Barron, Sofien Bouaziz, Dan B Goldman, Steven M Seitz, and Ricardo Martin-Brualla. Nerfies: Deformable neural radiance fields. In *Proceedings of the IEEE/CVF International Conference on Computer Vision*, pages 5865–5874, 2021.

Pascal Paysan, Reinhard Knothe, Brian Amberg, Sami Romdhani, and Thomas Vetter. A 3d face model for pose and illumination invariant face recognition. In *2009 sixth IEEE international conference on advanced video and signal based surveillance*, pages 296–301. Ieee, 2009.

Alec Radford, Luke Metz, and Soumith Chintala. Unsupervised representation learning with deep convolutional generative adversarial networks. *arXiv preprint arXiv:1511.06434*, 2015.

Katja Schwarz, Yiyi Liao, Michael Niemeyer, and Andreas Geiger. Graf: Generative radiance fields for 3d-aware image synthesis. *Advances in Neural Information Processing Systems*, 33:20154–20166, 2020.

Yichun Shi, Divyansh Aggarwal, and Anil K Jain. Lifting 2d stylegan for 3d-aware face generation. In *Proceedings of the IEEE/CVF conference on computer vision and pattern recognition*, pages 6258–6266, 2021.

J Ryan Shue, Eric Ryan Chan, Ryan Po, Zachary Ankner, Jiajun Wu, and Gordon Wetzstein. 3d neural field generation using triplane diffusion. In *Proceedings of the IEEE/CVF Conference on Computer Vision and Pattern Recognition*, pages 20875–20886, 2023.

Christian Szegedy, Vincent Vanhoucke, Sergey Ioffe, Jon Shlens, and Zbigniew Wojna. Rethinking the inception architecture for computer vision. In *Proceedings of the IEEE conference on computer vision and pattern recognition*, pages 2818–2826, 2016.

Qiuyu Wang, Zifan Shi, Kecheng Zheng, Yinghao Xu, Sida Peng, and Yujun Shen. Benchmarking and analyzing 3d-aware image synthesis with a modularized codebase, 2023a.

Tengfei Wang, Bo Zhang, Ting Zhang, Shuyang Gu, Jianmin Bao, Tadas Baltrusaitis, Jingjing Shen, Dong Chen, Fang Wen, Qifeng Chen, et al. Rodin: A generative model for sculpting 3d digital avatars using diffusion. In *Proceedings of the IEEE/CVF conference on computer vision and pattern recognition*, pages 4563–4573, 2023b.

Bin-Shih Wu, Hong-En Chen, Sheng-Yu Huang, and Yu-Chiang Frank Wang. Tpa3d: Triplane attention for fast text-to-3d generation. In *European Conference on Computer Vision*, pages 438–455. Springer, 2024.

Sijing Wu, Yichao Yan, Yunhao Li, Yuhao Cheng, Wenhan Zhu, Ke Gao, Xiaobo Li, and Guangtao Zhai. Ganhead: Towards generative animatable neural head avatars. In *Proceedings of the IEEE/CVF Conference on Computer Vision and Pattern Recognition*, pages 437–447, 2023a.

Yiqian Wu, Jing Zhang, Hongbo Fu, and Xiaogang Jin. Lpff: A portrait dataset for face generators across large poses. In *Proceedings of the IEEE/CVF International Conference on Computer Vision*, pages 20327–20337, 2023b.

Yang Xue, Yuheng Li, Krishna Kumar Singh, and Yong Jae Lee. Giraffe hd: A high-resolution 3d-aware generative model. In *Proceedings of the IEEE/CVF Conference on Computer Vision and Pattern Recognition*, pages 18440–18449, 2022.

Tarun Yenamandra, Ayush Tewari, Florian Bernard, Hans-Peter Seidel, Mohamed Elgharib, Daniel Cremers, and Christian Theobalt. i3dmm: Deep implicit 3d morphable model of human heads. In *Proceedings of the IEEE/CVF Conference on Computer Vision and Pattern Recognition*, pages 12803–12813, 2021.

Mihai Zanfir, Thieno Alldieck, and Cristian Sminchisescu. Phomoh: Implicit photorealistic 3d models of human heads. *arXiv preprint arXiv:2212.07275*, 2022.

Dingyun Zhang, Chenglai Zhong, Yudong Guo, Yang Hong, and Juyong Zhang. Metahead: An engine to create realistic digital head. *arXiv preprint arXiv:2304.00838*, 2023.

Mingwu Zheng, Hongyu Yang, Di Huang, and Liming Chen. Imface: A nonlinear 3d morphable face model with implicit neural representations. In *Proceedings of the IEEE/CVF Conference on Computer Vision and Pattern Recognition*, pages 20343–20352, 2022.

Xingran Zhou, Bo Zhang, Ting Zhang, Pan Zhang, Jianmin Bao, Dong Chen, Zhongfei Zhang, and Fang Wen. Cocosnet v2: Full-resolution correspondence learning for image translation. In *Proceedings of the IEEE/CVF conference on computer vision and pattern recognition*, pages 11465–11475, 2021.

Yiyu Zhuang, Hao Zhu, Xusen Sun, and Xun Cao. Mofanerf: Morphable facial neural radiance field. In *European Conference on Computer Vision*, pages 268–285. Springer, 2022.

Zi-Xin Zou, Zhipeng Yu, Yuan-Chen Guo, Yangguang Li, Ding Liang, Yan-Pei Cao, and Song-Hai Zhang. Triplane meets gaussian splatting: Fast and generalizable single-view 3d reconstruction with transformers. In *Proceedings of the IEEE/CVF conference on computer vision and pattern recognition*, pages 10324–10335, 2024.

Qi Zuo, Yafei Song, Jianfang Li, Lin Liu, and Liefeng Bo. Dg3d: Generating high quality 3d textured shapes by learning to discriminate multi-modal diffusion-renderings. In *Proceedings of the IEEE/CVF International Conference on Computer Vision*, pages 14575–14584, 2023.

Qi Zuo, Xiaodong Gu, Yuan Dong, Zhengyi Zhao, Weihao Yuan, Lingteng Qiu, Liefeng Bo, and Zilong Dong. High-fidelity 3d textured shapes generation by sparse encoding and adversarial decoding. In *European Conference on Computer Vision*, pages 52–69. Springer, 2024.

Supplementary Material

A Overview

This supplementary document provides additional materials to support the main paper "*HyPlaneHead: Rethinking Tri-plane-like Representations in Full-Head Image Synthesis*". It includes high-resolution qualitative comparisons, detailed explanations of the Near-Equal-Area Warping and Hy-Plane (2+2) representation. Additionally, we provide a video and key code snippets for reference.

B High-Resolution Qualitative Comparison (Fig. 5)

Due to the page limit of the paper, we were only able to include a low-resolution version of the qualitative comparison (Fig. 5). To better demonstrate the advantages of our method in generating fine details, we provide a high-resolution version of Fig. 5.

Fig. 6 presents a high-resolution qualitative comparison with state-of-the-art methods. Each subfigure corresponds to the following representations: (a) Tri-plane representation from Chan et al. (2022). (b) Tri-grid representation from An et al. (2023). (c) Single spherical tri-plane representation from Li et al. (2024), where the white dashed box highlights a discontinuity in the hair region caused by seam artifacts. (d–e) Dual spherical tri-plane representation from Li et al. (2024). (f–j) Our proposed Hy-plane representation.

While both the tri-plane and tri-grid representations (a and b) yield rich details in front-views, they suffer from inherent symmetry artifacts due to their Cartesian coordinate projections. Specifically, (a) exhibits clear mirroring face artifacts on the back of the head, reflecting front-view facial attributes. Similarly, (b) shows excessive left-right symmetry in the rear view.

The single spherical tri-plane (c) addresses the symmetry issue by introducing a spherical projection. However, it introduces seam artifacts due to the discontinuity in the (θ, ϕ) warping at the boundary of the spherical feature map (as shown in the white-dashed box, where the hair texture is misaligned).

To mitigate these seams, the dual spherical tri-plane approach (d–e) introduces an additional orthogonal spherical tri-plane. While this effectively eliminates seam artifacts, it comes at the cost of increased parameter numbers. Moreover, when merging the two spherical tri-planes, the regions with the lowest feature density—i.e., the equatorial areas—are used to cover the high-density polar regions of the other plane. This results in reduced expressiveness for fine details such as hair textures and shape contours.

In contrast, our method employs the Hy-plane representation, which leverages the dense and even spatial feature distribution of the tri-plane, as well as its efficient representation of symmetric regions, to ensure high-fidelity detail reconstruction. At the same time, a spherical tri-plane is utilized to provide anisotropic representation for asymmetric areas, effectively eliminating mirroring artifacts. Furthermore, we introduce a novel near-equal-area sphere-to-square warping strategy that avoids seam artifacts without compromising detail preservation.

C Details of Near-Equal-Area Warping

The Near-Equal-Area Warping method ensures that each region of the spherical input is mapped onto the planar representation with approximately equal surface area, thus avoiding excessive distortion and eliminating seam artifacts. This warping strategy is implemented in two steps: first, we use the Lambert Azimuthal Equal-Area Projection (LAEA projection) to flatten the spherical surface into a circular domain while preserving area; second, we apply Elliptical Grid Mapping to transform the circle into a square domain, enabling efficient utilization of the square-shaped feature map.

To better understand our proposed Near-Equal-Area Warping, we provide additional details and illustrative diagrams in this supplementary material.

In the Lambert Azimuthal Equal-Area Projection, the south pole of the sphere is "opened" and then flattened into a circular domain centered at the north pole. During this unfolding process, the distances between latitude lines are adjusted such that the resulting circular projection maintains equal-area

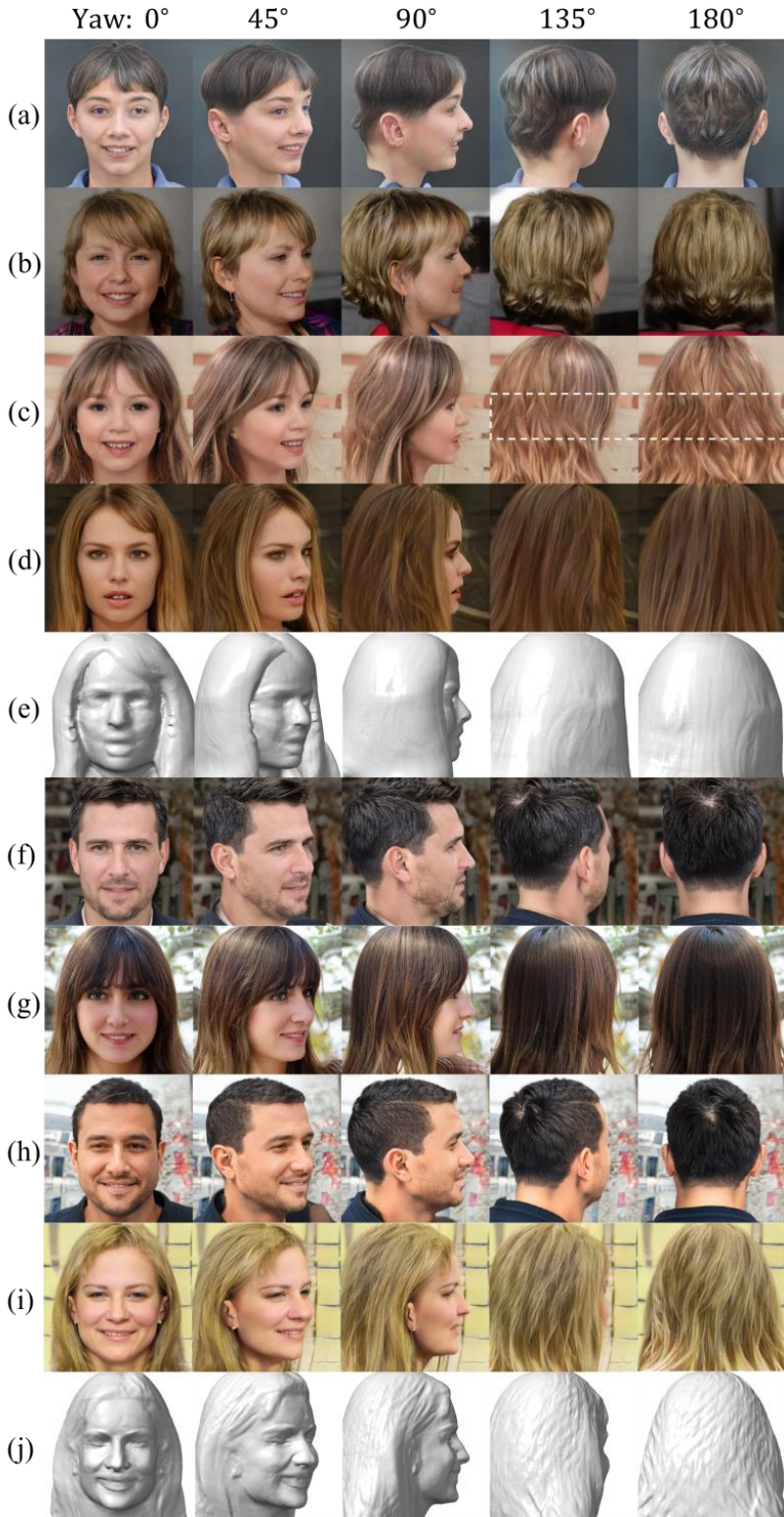


Figure 6: High-resolution qualitative comparison with state-of-the-art methods.

correspondence with the original spherical surface. A clearer understanding of this transformation can be gained from fig. 7. fig. 7(a-c) illustrates the dynamic process of the Lambert Azimuthal Equal-Area (LAEA) projection. fig. 7(d) illustrates the Lambert Azimuthal Equal-Area (LAEA)

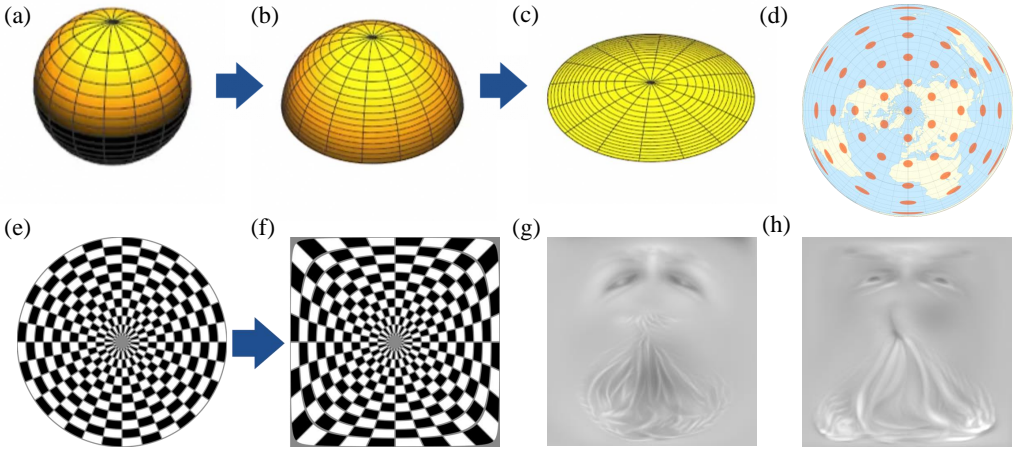


Figure 7: Illustrations of (a-d) the Lambert Azimuthal Equal-Area projection and (e-h) Elliptical Grid Mapping.

projection using a world map example, demonstrating that it preserves area. Each orange circle represents a region of equal size on the original spherical surface.

Subsequently, we employ Elliptical Grid Mapping to convert the circular domain into a near-equal-area square grid. Among various methods for transforming a circle into a square, we choose Elliptical Grid Mapping due to its following advantageous properties: 1. Approximate equal-area mapping: The variation in local area across the transformed plane is minimized. 2. Smooth central region and minimal distortion at the boundaries: This preserves important structural details, especially near edges. 3. Computationally simple and stable: It avoids division operations, which is crucial for maintaining gradient stability during training. An intuitive illustration of this mapping is provided in fig. 7. fig. 7(e,f) show the deformation of Elliptical Grid Mapping under black-and-white stripe patterns, indicating that most regions experience minimal area distortion. fig. 7(g,h) show the feature maps of the spherical plane before and after applying Elliptical Grid Mapping. Without this mapping, the model fails to effectively utilize the corner regions of the feature map. In contrast, with Elliptical Grid Mapping, most regions of the feature map are efficiently utilized.

For convenience, we have included the core implementation of the Near-Equal-Area Warping method in the supplementary material as `near_equal_area_warping.py`.

D Details of Hy-Plane (2+2)

Although the LAEA projection addresses seam artifacts, its implementation still requires "opening" the South Pole, which inherently leaves one remaining polar region. This region is more prone to high-frequency noise and distortion.

While in the Hy-Plane (3+1) formulation we can hide the problematic area by orienting it downward, this approach limits the generality of our representation, particularly for objects or scenes that require rendering from all directions. In such cases, relying on a single hidden region is insufficient, as any arbitrary viewpoint may expose the problematic area and lead to visible artifacts. To make the Hy-Plane representation more universally applicable, we propose Hy-Plane (2+2) to resolve this issue.

The Hy-Plane (2+2) representation combines two planar planes (P_{XY} and P_{YZ}) and two spherical planes (P_a and P_b). These two spherical planes overlap spatially but are oriented such that their respective South Poles face opposite directions. Specifically, as shown in main paper Fig. 3 (d), the North Pole of P_a is oriented along the negative z -axis, while the North Pole of P_b is oriented along the positive z -axis; consequently, their South Poles point in opposite directions. By assigning weights to each plane and summing them, the smooth North Polar regions of one spherical plane can effectively

cover the problematic South Polar regions of the other, thereby eliminating the distortion-prone areas entirely.

E More Qualitative Results

Below are additional qualitative results comparing our method with existing approaches on a larger set of examples. These include variations in pose, expression, and lighting conditions.



Figure 8: Additional qualitative results.